NASA/TM—1998-206632

Performance of an Axisymmetric Rocket Based Combined Cycle Engine During Rocket Only Operation Using Linear Regression Analysis

Timothy D. Smith and Christopher J. Steffen, Jr.
Lewis Research Center, Cleveland, Ohio

Shaye Yungster
Institute for Computational Mechanics in Propulsion, Cleveland, Ohio

Dennis J. Keller
RealWorld Quality Systems Inc., Rocky River, Ohio

National Aeronautics and
Space Administration

Lewis Research Center

March 1998

Available from

PERFORMANCE OF AN AXISYMMETRIC ROCKET BASED COMBINED CYCLE ENGINE DURING ROCKET ONLY OPERATION USING LINEAR REGRESSION ANALYSIS

Timothy D. Smith
Christopher J. Steffen, Jr.
National Aeronautics and Space Administration
Lewis Research Center
Cleveland, Ohio

Shaye Yungster
Institute for Computational Mechanics in Propulsion
Cleveland, Ohio

and

Dennis J. Keller
RealWorld Quality Systems Inc.
Rocky River, Ohio

SUMMARY

The all rocket mode of operation is shown to be a critical factor in the overall performance of a rocket based combined cycle (RBCC) vehicle. An axisymmetric RBCC configuration was used to determine specific impulse efficiency values based upon both full flow and gas generator cycles. Design of experiments methodology was used to construct a test matrix and multiple linear regression analysis was used to build parametric models. The main parameters investigated in this study were: rocket chamber pressure, rocket exit area ratio, injected secondary flow, mixer-ejector inlet area ratio, mixer-ejector area ratio, and mixer-ejector length-to-inlet diameter ratio. A perfect gas computational fluid dynamics analysis, using both the Spalart-Allmaras and k-ε turbulence models, was performed with the NPARC code to obtain values of vacuum specific impulse. Results from the multiple linear regression analysis showed that for both the full flow and gas generator configurations increasing mixer-ejector area ratio and rocket area ratio increase performance, while increasing mixer-ejector inlet area ratio and mixer-ejector length-to-diameter ratio decrease performance. Increasing injected secondary flow increased performance for the gas generator analysis, but was not statistically significant for the full flow analysis. Chamber pressure was found to be not statistically significant.

INTRODUCTION

For many years rocket-based combined cycle (RBCC) engine systems have been envisioned as the means to achieve affordable single-stage-to-orbit (SSTO), references 1 to 7. The inherent advantage to RBCC engine systems is the increased specific impulse, or fuel efficiency brought about by the airbreathing part of the system as compared to an all rocket SSTO vehicle. A more fuel efficient engine system will increase the vehicle payload mass fraction and thus reduce the cost-per-pound to orbit. A typical RBCC engine will operate in four modes; (1) ejector ramjet, (2) ramjet, (3) scramjet, and (4) all-rocket. In general, the performance of the rocket is based on the design chamber pressure, mixture ratio, propellants, and exit area ratio of the engine. But, for most RBCC systems the rocket is simply a subset of the engine. While a significant amount of analysis has been performed on modes 1 to 3, including some computational fluid dynamics studies (ref. 8), very little analysis has been performed on mode 4. However, the performance of an RBCC system in mode 4 can have a significant affect on total system performance.

The rockets are used during two modes of operation, ejector ramjet for lift-off and all-rocket for orbit insertion. To accomplish the ejector pumping in mode 1, the rockets are generally located in the forward section of the engine (fig. 1(a)) followed by a mixer-ejector section. This section can be round, square, straight, or diverging with a single rocket or multiple rockets. While this configuration works well for mode 1, it is not ideal for the all-rocket mode 4 performance. In mode 4 the mixer-ejector section can be viewed effectively as

a nozzle for the rocket. The most noticeable feature of the mode 4 configuration is the discontinuity between the rocket nozzle exit and the mixer-ejector section. Due to this configuration, the potential exists for free expansion losses as the flow moves from the rocket nozzle exit to mixer-ejector wall. The plume impinges on the walls creating a series of reflected shocks inside the engine. The flow path is significantly different from an optimum rocket nozzle with the same overall expansion area ratio. Over the years a significant amount of work has been performed on developing methods for designing optimal rocket nozzles, figure 1b (refs. 9 and 10). However, there is a lack of design or analysis for an RBCC system operating in a mode 4 configuration.

The objective of the present study is to quantify the effects of the mixer-ejector section on the all-rocket mode performance. A Navier-Stokes, perfect gas computational fluid dynamics (CFD) analysis was performed using the NPARC (ref. 11) computer code. An axisymmetric model, which consisted of a single rocket engine with a variable duct, was chosen for ease of modeling. This model encompasses the most influential parameters which affect the flowfield and the impact on performance. The main parameters investigated in this study were: chamber pressure, rocket area ratio, injected secondary flow, mixer-ejector inlet area, mixer-ejector area ratio, and mixer-ejector length-to-inlet diameter. The CFD calculations were used to assess the specific impulse efficiencies of the various RBCC configurations studied. Design of experiments (DOE) was used to set up the test matrix and a linear statistical regression model was created based upon the CFD results.

SYMBOL LIST

A^*	Rocket throat area (in^2)
A_3	Mixer-ejector inlet area (in^2)
A_6	Mixer-ejector exit area (in^2)
D	Vehicle drag (lb$_f$)
D_3	Mixer-ejector inlet diameter (in)
E	Statistical model error term (percent)
FF	Results from full-flow analysis
F	Thrust (lb$_f$)
F_{CFD}	Thrust from CFD results (lb$_f$)
g_o	Gravitational constant (32.174 lb$_m$ -ft/ lb$_f$ -sec^2)
GG	Results from gas-generator analysis
Isp	Specific impulse (sec)
Isp$_{CFD}$	Specific impulse from CFD results (sec)
Isp$_{isentropic}$	Specific impulse from isentropic calculations (sec)
k-ε	k-ε turbulence model
L	Mixer-ejector length (in)
$\dot{m}_p$	Primary rocket mass flow (lb$_m$/sec)
$\dot{m}_s$	Injected secondary flow (lb$_m$/sec)
m_s	Percent injected secondary flow, $\left(\dfrac{\dot{m}_s}{\dot{m}_p} \times 100 \right)$
$\dot{m}_t$	Total mass flow (lb$_m$/sec)
N	Number of data points used in the multiple linear regression
NSS	Regression coefficient is not statistically significant
P	Number of terms in the final statistical model
Pc	Rocket engine chamber pressure (psia)
p_e	Mixer-ejector exit static pressure (lb$_f$/in^2)
q	Dynamic pressure (lb$_f$/ft^2)
R^2	Residual error term
SA	Spalart-Allmaras turbulence model
$S_{Y.X}$	Goodness of fit statistic between experimental value and model prediction
t	Multiplicative statistical constant dependent upon N-P
u_6	Mixer-ejector axial exit velocity (ft/sec)
x_i	Statistical model independent variable
x_{imin}	Statistical model independent variable—minimum value possible
x_{imax}	Statistical model independent variable—maximum value possible
X_i	Statistical model input transformed variable
Y_i	Calculated Isp for statistical model.

| $\overline{Y}$ | Mean calculated Isp for statistical model |
| $\hat{Y}_i$ | Predicted value of the output variable from statistical model |

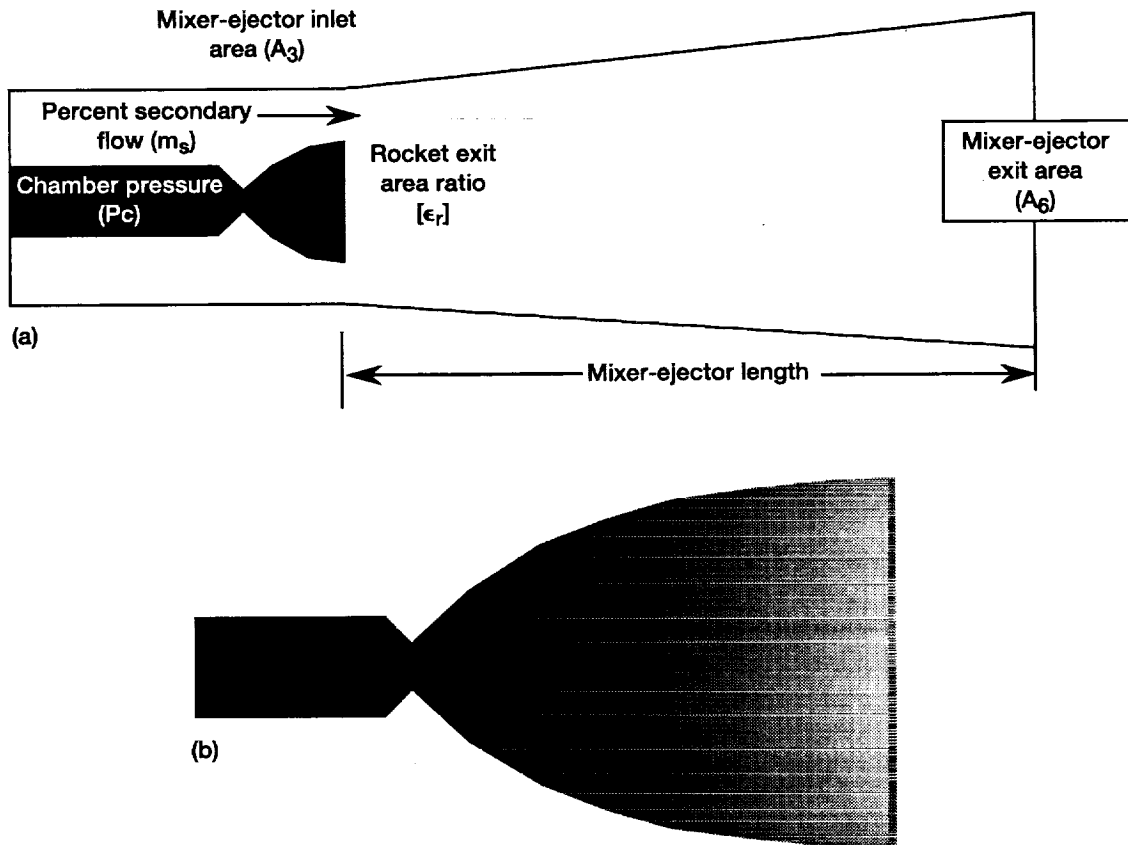| β | Statistical model coefficient |
ΔV_f	Incremental actual flight velocity (ft/sec)
ε_{ME}	Mixer-ejector nozzle exit area ratio
ε_r	Rocket nozzle exit area ratio
η_{Isp}	Specific impulse efficiency (percent)
ρ	Density (lb_m/ft^3)
Θ	Vehicle flight path angle with respect to horizontal (degrees)

Figure 1.—(a) Axisymmetric RBCC engine configuration. (b) Optimized rocket nozzle configuration.

BACKGROUND

System Performance

For RBCC systems, the equivalent effective specific impulse, or I*, is the integrated value which is representative of total system performance. As seen in figure 2 (ref. 6), for a SSTO vehicle I* can have a range of 500 to 750 sec, while an all rocket system is limited to 320 to 380 sec. Due to the increase in I*, mass fractions of 0.20 to 0.35 are achievable for RBCC systems, while an all-rocket SSTO has a mass fraction limit of only 0.10. The increased mass fraction allows for more payload, a more robust vehicle structure, and a lower cost per pound to orbit.

When analyzing the specific impulse of a combined cycle engine, the main figure of merit is I* or the equivalent effective specific impulse. I* takes into account gravity, vehicle drag, and thrust to provide a constant value that can be used to yield the proper vehicle mass ratio. It is calculated as the integral with respect to flight velocity of the effective specific impulse (I_{eff}), from reference 6.
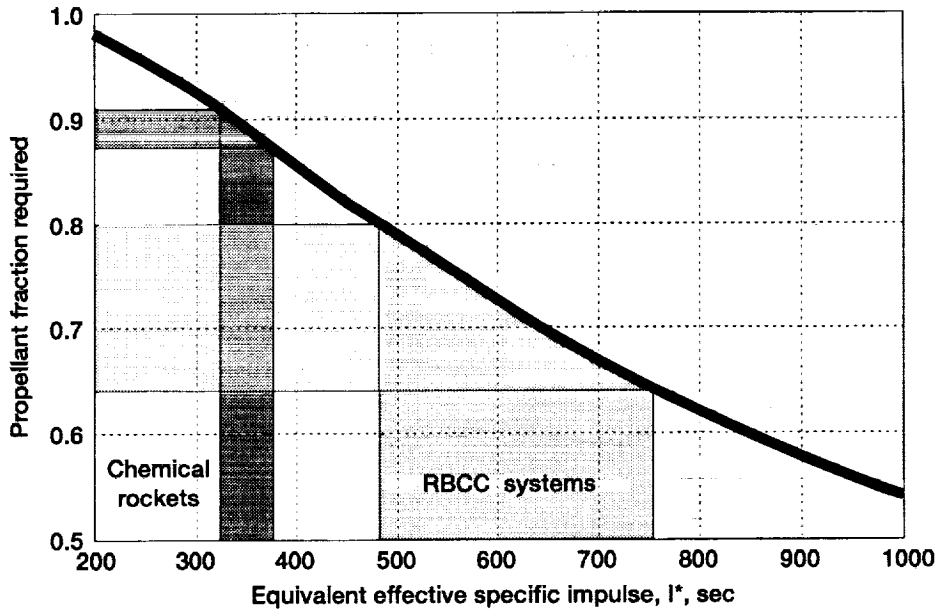
Figure 2.—Vehicle propellant mass fraction as a function of equivalent effective specific impulse (I*).

$$I^* = \frac{\Delta V_f}{\int \frac{dv}{I_{eff}}} \qquad (1)$$

$$I_{eff} = I_{sp}\left[1 - \frac{W\sin\Theta}{T} - \frac{D}{T}\right] \qquad (2)$$

I* can also be calculated in terms of vehicle mass ratios (ref. 6):

$$I^* = -\frac{\Delta V_f}{g_o\ln\frac{M_o}{M_1}} = -\frac{\Delta V_f}{g_o\ln\left(1 - \frac{M_p}{M_1}\right)} \qquad (3)$$

During the first three modes of operation, an RBCC system can achieve net Isp values over 3500 sec, before dropping off to near 450 sec for the all rocket mode. Figure 3 shows a representative figure of how Isp varies as a function of Mach number over a given trajectory. The results are based upon a constant dynamic pressure trajectory for a vehicle with the following characteristics:

Required ΔV_f	25,150	sec
Vehicle mass (M_o)	30,000	lb_m
Design I*	500	sec
Rocket mode Isp	460	sec
Dynamic pressure (q)	1,250	lb_f/ft^2

Several system effects can be determined by a careful examination of the figure. Obviously, increasing performance of the airbreathing modes will allow for a lower performing rocket system at a constant I*. Conversely, as I* is increased, the Isp from the airbreathing mode must be increased if the rocket is at the maximum Isp attainable. The same constant I* can also be achieved by extending the ΔV_f of the airbreathing portion of the trajectory, hence extending the scramjet to all-rocket transition to a higher Mach number. However, increasing the scramjet to all-rocket transition Mach number also increases the amount of convective
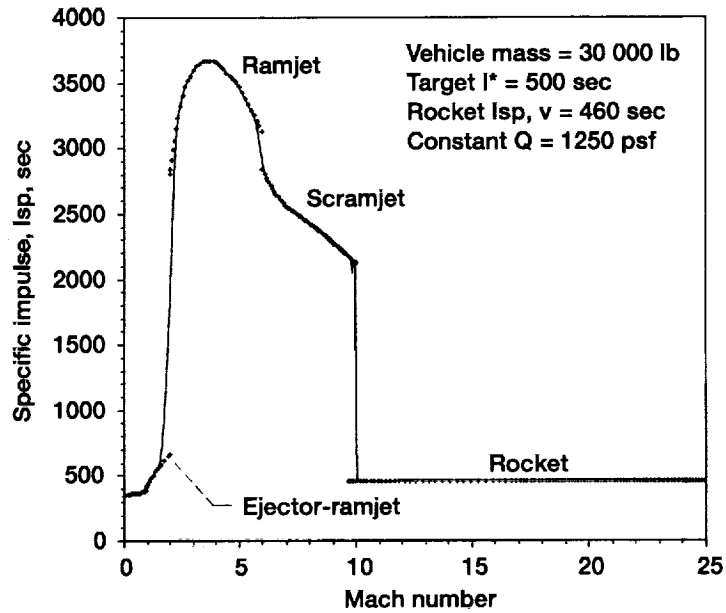
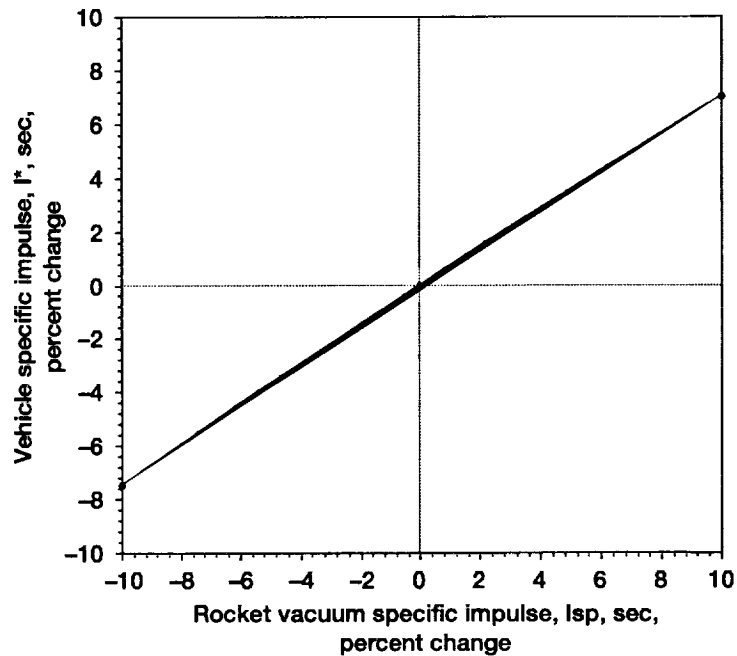Figure 3.—Specific impulse versus Mach number for an RBCC trajectory during the four modes of operation.

Figure 4.—Percent change in I* as a function of a percent change in rocket Isp.

heating the vehicle must withstand, thus requiring a vehicle utilize advanced thermal protection materials or an active cooling system. Either option is expensive and adds vehicle mass which reduces the payload-to-orbit capability. As a result, a balance must be reached between total I* and the vehicle cooling capacity.

Figure 4 shows the result of how varying rocket Isp affects vehicle I*, as calculated using equation 1. The same vehicle and sample trajectory that were used to create figure 3 was used to create figure 4. Starting with a baseline rocket Isp = 460 sec., rocket mode Isp was varied by ±10% and I* was then recalculated. The results show that a 10% loss in rocket mode Isp will reduce I* by over 7%, a gain in rocket mode Isp of 10%

will provide an I* increase of over 7%. As a result any change in rocket mode Isp has a significant effect on overall system performance. I* becomes slightly less sensitive to rocket mode Isp for vehicles with higher design I* values.

This relationship between rocket mode Isp and I* is important when performing system trade studies like those found in references 12 and 13. As shown in figure 4, the delivered performance of mode 4 will impact the total system performance I*. The changes in total I* will then affect how the engine system and vehicle are configured to accomplish the performance goals of modes 1 to 3. Other factors affected by the impact that mode 4 performance has on the system include trajectory issues like flight dynamic pressure and the Mach number transition point between modes 3 and 4. All of these trades eventually impact the vehicle size, mass, obtainable payload to orbit and cost. Therefore, given the potential system effects, it is imperative that there is an accurate assessment of mode 4 performance.

Rocket Nozzles

For an RBCC vehicle, mode 4 vacuum Isp is based on the total exit area ratio of the engine which usually includes the vehicle aft body. The total exit area ratio for these systems is generally very high, 500 to 1000. The all rocket SSTO systems are hampered by the physical size needed to obtain high area ratios and the relative low performance of the rockets in the atmospheric portions of flight. Because most rocket nozzles are single point designs, a compromise design is used to balance performance at sea level through orbit insertion. As a result, the design area ratio is only optimal for a very narrow portion of the flight. At sea level the flow is slightly over expanded, while at altitude the flow is underexpanded. An alternative to conventional rocket nozzle designs are aerospike nozzles which can obtain high relative area ratios (ref. 14). These nozzles differ from conventional rocket nozzles by turning the exhaust gases radially inward towards the axis of the spike. Because there is no outer plume boundary, the expansion process is controlled by the ambient pressure, as a result these types of nozzles are less susceptible to over-expansion and under-expansion. Aerospike nozzles are expected to increase performance due to altitude compensation, thus running a near optimum performance over the entire ascent trajectory. However, the overall performance will not reach the very high Isp levels of an RBCC system

Using the following example to define a typical rocket, ideal Isp can be calculated over a range of total exit area ratios with a finite area combustor using the one-dimensional equilibrium Chemical Equilibrium Composition (CEC) computer code (ref. 15):

Propellants: Gaseous Oxygen and Gaseous Hydrogen
Chamber Pressure: 1200 psia
Mixture Ratio: 6.0

Figure 5 shows Isp as a function of area ratio which represents the maximum ideal values attainable using a nozzle such as the one shown in figure 1b. As the area ratio goes beyond 150, the ideal Isp grows very slowly to 509 sec at an area ratio of 1000. Obviously these numbers are not practical due to a variety of loss mechanism present in any nozzle configuration. Previous studies (refs. 12 to 16) have used a value of 470 sec for rocket mode performance when examining RBCC engines. This results in specific impulse efficiencies on the order of 92 to 96% depending upon total area ratio available for a conventional nozzle. Experimental programs have shown that very high specific impulse efficiencies (96 to 98%) are possible with nozzle area ratios up to 1025:1 (refs. 17 and 18).

One of the main differences between mode 4 of an RBCC system and a conventional rocket engine is the initial expansion of the rocket flow into the mixer-ejector section. Unlike a conventional nozzle, the rocket exhaust must cross the inlet cavity where there is no direct nozzle surface for the flow to act upon, resulting in a loss of thrust. The initial expansion of the rocket exhaust is controlled by the Prandtl-Meyer expansions, which is a function of the rocket area ratio, nozzle exit divergence angle, exit Mach number, and exit static pressure. Because of the severe expansion angle, the rocket exhaust intersect with the mixer-ejector wall at a very steep angle resulting in strong reflected shocks in the mixer-ejector. These shocks cause a loss of total pressure and momentum, resulting in a loss of thrust and engine efficiency. To alleviate the losses from the free expansion, the cavity upstream of the rocket can be pressurized. This would reduce the expansion angle and possibly limit the strength of the reflected shock and provide a smooth transition for rocket flow attachment to the mixer-ejector wall. As discussed in reference 1, several system configurations exist which utilize secondary flow for the cavity pressurization. If the inlet is left open, ram air could still flow into the cavity, however this may result in significant ram drag and the system may not be able to capture enough flow at
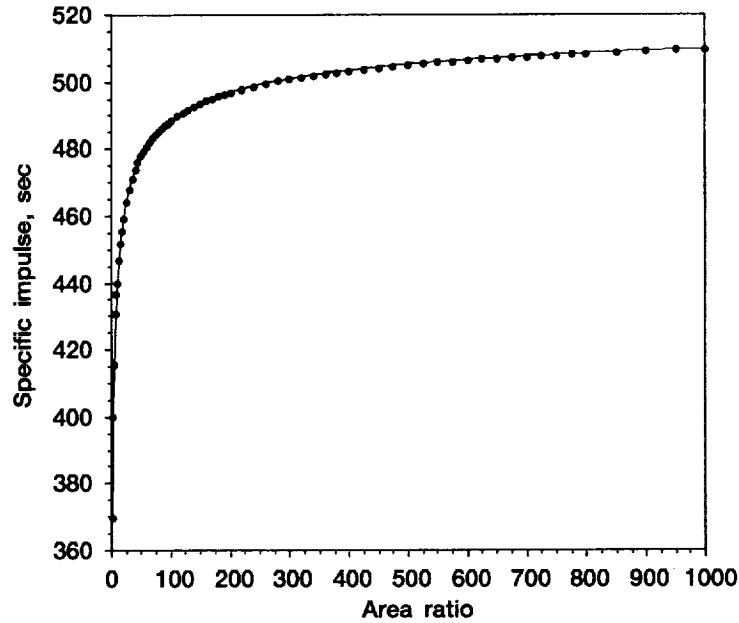
Figure 5.—Ideal specific impulse versus rocket area ratio for a hydrogen/oxygen rocket engine (chamber pressure = 1200 psia, mixture ratio = 6).

higher altitudes. A second method would be to pressurize the cavity with flow from fluids carried on the vehicle. This secondary gas could come from the rocket engines using a gas generator cycle or from propellants carried to cool engine and vehicle surfaces.

A limited amount of work has been conducted to examine the effects of secondary flow on rocket nozzles (ref. 19). In that program cold-flow experiments with air and carbon tetrafluoride were performed where secondary flow was introduced through a plenum surrounded by a shroud around the exit of a 1/16 scale J-2 rocket nozzle. The J-2 nozzles had an exit area ratio of 27.2:1, with both cylindrical and conical shrouds out to an area ratio of 55:1. The secondary flow was shown to raise the thrust coefficient of the system for both types of shrouds, with the conical configuration having the higher performance. The experiment also showed that increasing length resulted in lower performance for the cylindrical configuration. Results from that work show that secondary flow is a possible solution for increasing nozzle performance.

AXISYMMETRIC CONFIGURATION

An axisymmetric geometry was used for this analysis (fig. 1(a)). The system consists of a single rocket engine in the forward section of a mixer-ejector duct. The Rao nozzle design code (ref. 20) was used to design the nozzle contours for each rocket area ratio. The following baseline parameters were assumed for each case:

Propellants:	Gaseous Oxygen and Gaseous Hydrogen
Ratio of Specific Heats (γ)	1.2
Mixture Ratio	6.0

Table I presents the main RBCC engine parameters investigated in this study.

TABLE I.—RBCC ENGINE PARAMETERS AT THREE LEVELS

Chamber pressure (P_c)(psi)	300	750	1200
Rocket area ratio (ε_R)	4	12	20
Percent of secondary flow (m_s)	0.0	4.0	8.0
Mixer-ejector inlet area ratio[A_3/A^*]	40	120	200
Mixer-ejector area ratio [A_6/A_3](ε_{ME})	1.0	1.5	2.0
Mixer-ejector length-to-diameter [L/D_3] ratio.	2.0	3.5	5.0

Figure 1(a) shows the parameters varied for this study. The mixer-ejector inlet area ratio (A_3/A^*) is the total area at the beginning of the mixer-ejector divided by the area of the rocket engine throat area. The mixer-ejector area ratio is the amount of expansion provided by the mixer-ejector only (A_6/A_3). The percentage of injected secondary flow (m_s) is in relation to the primary rocket flow.

The measure of performance used in this analysis is specific impulse efficiency. To calculate specific impulse, the CFD results were used to calculate mass flow and thrust with a trapezoidal integration across at the mixer-ejector exit plane, equations 1 and 2 respectively. In this analysis ambient pressure outside of the nozzle was set to simulate vacuum conditions. As a result, the effect of ambient pressure on thrust is negligible. The values were then used to calculate the specific impulse, equation 3:

$$\dot{m}_t = \int_{EXIT} (\rho u_6) dA_6 \tag{4}$$

$$F = \int_{EXIT} (\rho u_6^2 + p_6) dA_6 \tag{5}$$

$$Isp_{CFD} = \frac{F}{\dot{m}_t} \tag{6}$$

The calculated Isp results from the CFD analysis were compared to the Isp values from isentropic flow calculations which represent the theoretical ideal performance levels.

$$\eta_{Isp} = \frac{Isp_{CFD}}{Isp_{Isentropic}} \tag{7}$$

Combustion efficiency is assumed to be 100% for all cases. Ideal performance is based on expanding the flow to maximum area ratio available at the mixer-ejector exit.

CFD ANALYSIS

The flow solver chosen for this study was NPARC v3.0 (ref. 11). NPARC is a multidimensional flow simulator used for a wide variety of fluid flow analysis within the aerospace community. NPARC is a perfect gas, finite difference code for structured, and multiblock grids. The cases assumed steady, axisymmetric, turbulent flow through the RBCC engine. Two turbulence models were investigated: the Spalart-Allmaras (SA) 1-equation model (ref. 21) and the Chien k–ε 2-equation model (ref. 22) with Sarkar's compressibility correction (ref. 23). The effect of the two different turbulence models upon integral quantities such as net thrust and net massflow will be discussed in a later section. A more detailed discussion of the CFD modeling can be found in reference 24.

The physical boundaries of the RBCC system have been modeled as standard adiabatic, no-slip surfaces. The combustion chamber was simulated by specifying the constant total conditions given in Table I. The total conditions were obtained by running a one-dimensional equilibrium (CEC) code (ref. 13) for a given chamber pressure, with ambient temperature gaseous hydrogen and gaseous oxygen as propellants at a mixture ratio of 6.0. As a result, the ratio of specific heats (γ) was assumed to be a constant 1.2 for all CFD analysis. The secondary flow was modeled as a fixed massflux boundary with a total temperature of 1600 °R which is based on a rocket pre-burner conditions.

TABLE II.—CFD CONSTANT TOTAL CONDITONS FROM A
CHEMICAL EQUILIBRIUM CODE

Chamber Pressure (psia)	Molecular Weight	Chamber Temperature (°R)
300	13.02	6200
750	13.19	6400
1200	13.27	6500

Great care was taken to insure the CFD results were insensitive to grid convergence with proper spatial resolution. A grid sensitivity study was performed which showed that the results were insensitive to grid size. A

detailed discussion of the mesh generation methodology and NPARC configuration can be found in reference 24.

DESIGN OF EXPERIMENTS AND REGRESSION STRATEGY

The DOE analysis matrix was developed to reduce the number of CFD cases required to develop a parametric performance model. To fully model all linear effects, curvilinear effects, bilinear effects, and potential interactions a total of 729 (i.e. 3^6) cases would have been required; a prohibitively resource intensive number of cases. Using DOE, the full matrix was reduced to a total of 36 CFD cases; enough to examine the linear effects, curvilinear effects, bilinear effects, and interactions. The 36 CFD case model was further reduced to nine CFD cases to examine only the linear effects. Results from the linear analysis provides a good first order estimate of which parameters have the most significant impact on performance and if that impact is positive or negative. The linear model forms an unreplicated 2^{7-4} fractional factorial design augmented with a single centerpoint. This is an efficient design that permits an investigation of linear effects of up to 7 variables in only 8 experiments. A ninth CFD case, the centerpoint, was added as a preliminary check on the assumptions of linearity. It is a 1/16 (i.e. 2^{-4}) fraction of a full 128 (i.e. 2^7) term model. This design quantifies the linear effects of the six input variables with the assumption that there are no curvilinear effects, no bilinear effects, and no interactions between the input variables. Table III lists the detailed configuration for each of the nine cases in the model along with the total area ratio $(A_6/A_3 * A_3/A^* = A_6/A^*)$ as a reference.

TABLE III.—AUGMENTED FRACTIONAL FACTORIAL DESIGN INPUT VARIABLES

Case	Chamber Pressure (psi)	Secondary Flow Percent	Mixer Inlet Area Ratio	Length to Dia. Ratio	Mixer Area Ratio	Rocket Area Ratio	Total Area Ratio
	x_1	x_2	x_3	x_4	x_5	x_6	
1	300	8.0	40.0	2.0	2.0	4.0	80
2	300	0.0	40.0	5.0	2.0	20.0	80
3	1200	0.0	200.0	2.0	2.0	4.0	400
4	300	0.0	200.0	5.0	1.0	4.0	200
5	300	8.0	200.0	2.0	1.0	20.0	200
6	1200	8.0	200.0	5.0	2.0	20.0	400
7	1200	8.0	40.0	5.0	1.0	4.0	40
8	1200	0.0	40.0	2.0	1.0	20.0	40
9	750	4.0	120.0	3.5	1.5	12.0	180

A multiple linear regression (MLR) analysis was performed for each set of Isp efficiencies to determine the effect each variable had on performance. The statistical design and analysis was performed with the RS/CLIENT™ software. The current model assumes all relationships are significant and the main effects are accurate. For each data set a simple relationship is based on the input variables. Each variable in the MLR has an associated coefficient.

$$\eta_{Isp} = \beta_0 + \beta_1 X_1 + \beta_2 X_2 \dots + \beta_6 X_6 \tag{8}$$

Positive coefficients will increase performance while negative coefficients will decrease performance. For the current analysis the variables were normalized to values of -1 and +1 so the estimated coefficients would reflect the relative strengths of the effects. Hence, the larger a coefficient value the greater its influence on the final result. As a result, the X_i variable is actually:

$$X_i = \frac{X_i - \left(\dfrac{X_{imax} + X_{imin}}{2}\right)}{\dfrac{X_{imax} - X_{imin}}{2}} = \frac{x_i - \text{midpoint}}{\text{range}/2} \tag{9}$$

In a typical MLR, significance is identified and quantified relative to an estimate of system noise based on a number of repeated experiments. However, a computer code should generate an insignificant level of noise and repeating each case should generate the same answer. Therefore, unlike experimental efforts, repeat-

ing a CFD case does not add another degree of freedom to the statistical analysis. As a result, the error (E) estimates presented use an artificial noise term generated with the residual term (R^2) calculated from fitting 9 data points to a 7 term model. The reader is encouraged to examine reference 24 for a discussion on the steps taken to insure that the results did not suffer from grid dependence, incomplete convergence, or numerical instability.

Along with the MLR results are the values for residual (R^2), goodness of fit $S_{Y.X}$, and an error estimate (E). The $S_{Y.X}$ is a goodness of fit statistic which summarizes the agreement between the actual output value and the associated model predictions.

$$R^2 = \frac{\sum\left(\hat{Y}_i - \overline{Y}\right)^2}{\sum\left(Y_i - \overline{Y}\right)^2} \tag{10}$$

$$S_{Y.X} = \sqrt{\frac{\sum\left(Y_i - \hat{Y}_i\right)^2}{(N-P)}} \tag{11}$$

$S_{Y.X}$ may be used to calculate approximate prediction errors (E) as follows.

$$E \approx t \times S_{Y.X} \tag{12}$$

where t is a multiplicative constant that changes depending on the residual degrees of freedom (N-P). These t-constants can be located in any statistical text or mathematical handbook under t-distribution, reference 25. This error term is the variation in predicted results at a given point, with 95% confidence.

RESULTS AND ANALYSIS

CFD Results

For a more detailed discussion of the CFD analysis the reader is encouraged to examine reference 24. However, a brief summary is included in the following section to highlight some of the flow characteristics which affect system performance. Figure 6 shows a representative Mach number distribution for case 7 with the Spalart-Allmaras turbulence model. Just downstream of the rocket nozzle exit is the free expansion of the plume to the mixer-ejector wall. The plume consists of both a shear layer and oblique shock structure. Next, the rocket expansion impinges onto the mixer-ejector wall. As the flow tries to turn parallel to the wall, a re-flected oblique shock is created which propagates toward the centerline as the flow moves downstream. In some cases, the mixer-ejector is short enough that the oblique shocks do not meet at the center line, but cross the nozzle exit plane before colliding. However, if the duct is long enough, the oblique shocks meet at the centerline, propagate downstream to re-impinge on the wall, creating a diamond like structure in the flow. Also, as seen in the plot, when the oblique shocks impinge upon the wall, shock induced boundary layer separations are formed. Weak secondary expansion and shock waves can also be seen in the flow. Substantial boundary layer growth is also present in many of the solutions, especially for the longer mixer-ejectors. All cases exhibit some flow stratification and flowfield divergence at the mixer-ejector exit.
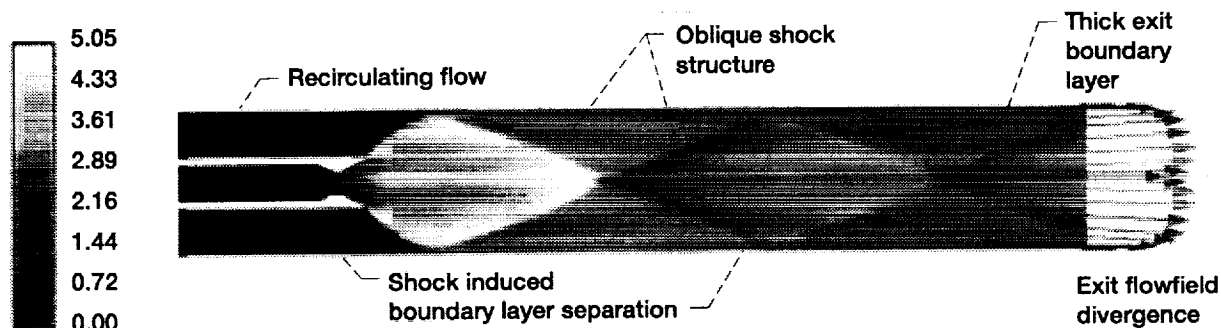

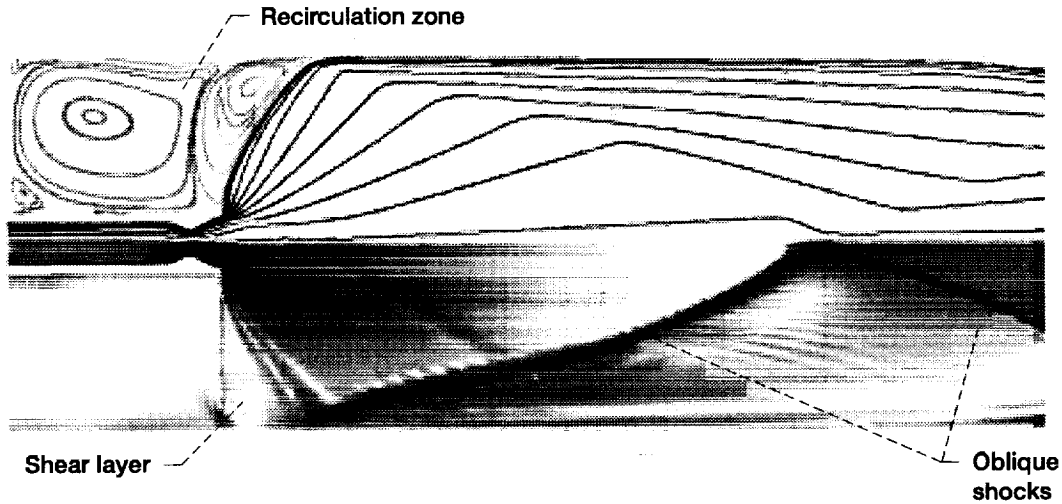Figure 6.—Mach contour plot for case 7.

Figure 7.—Particle trace for case 4 with zero injected secondary flow, showing the cavity recirculation zone.
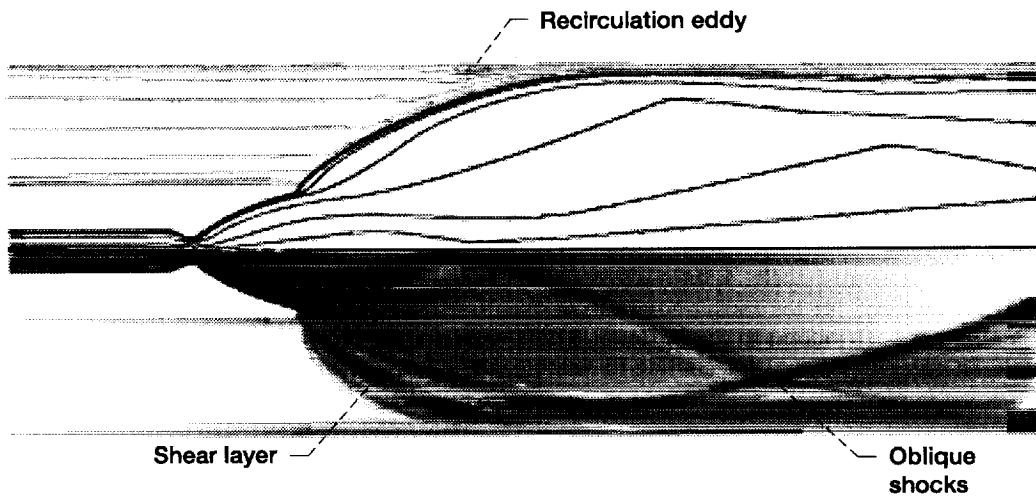

Figure 8.—Particle trace for case 5 with 8.0% injected secondary flow, showing only a small cavity recirculation zone near the wall impingement.

A primary concern in this configuration is how the free expansion from the rocket nozzle exit to the mixer ejector wall affects overall performance. Figure 7 is a composite picture showing a particle trace plot on top and a numerical Schlieren image on the bottom from case 4 where no additional secondary flow is injected and the system acts as a supersonic driven cavity. As can be seen from the particle traces, several recirculation zones are present inside of the cavity. The numerical Schlieren provides an excellent view of the shear layers and reflected oblique shock structures. Figure 8 from case 5 is also a composite picture showing a particle trace plot on top and a numerical Schlieren image on the bottom shows. From the particle trace it is obvious that when secondary flow is added that there is almost no recirculation zone, only one small eddy is present near the impingement point of the primary stream. The numerical Schlieren provides an excellent view of the shear layers and reflected oblique shock structures, especially the change in exit angle of the exhaust plume from the rocket engine. Obviously the figures demonstrate that changes in the parameters have a dramatic effect on the physical flow field. However, it is up to the regression analysis to determine which changes affect performance and if the changes lead to a higher performing system.

Table IV presents the results from specific impulse calculations for the CFD cases:

TABLE IV.—SPECIFIC IMPULSE CALCULATIONS
FROM CFD CASES

Case	Spalart-Allmaras Isp (sec)	k–ε Isp (sec)
1	399.54	410.42
2	424.33	427.06
3	415.94	415.88
4	361.73	373.85
5	411.29	425.22
6	430.64	437.21
7	374.07	375.30
8	416.89	418.70
9	418.36	423.38

Due to the presence of secondary flow, there are two methods to calculate the ideal performance, each is based upon a different assumed system cycle. The first method is to base the ideal performance on a full-flow cycle (Isp_{FF}) where the ideal performance is based on the rocket flow only ($\dot{m}_p = \dot{m}_t$). Specific impulse can be calculated from equation 6 and substituting for the mass flow to obtain:

$$Isp_{FF} = \frac{F}{\dot{m}_p} \qquad (13)$$

In a full-flow system all of the propellants available are routed to the rocket engine where they are mixed and burned. Any flow not consumed by the rocket is considered a loss. In this analysis the secondary bleed flow ($\dot{m}_s$) is a loss. The second method of comparison to a gas generator type of system (Isp_{GG}) is shown by equation 14.

$$Isp_{GG} = \frac{F}{\dot{m}_p + \dot{m}_s} \qquad (14)$$

In a typical gas generator cycle, additional propellant is required to power the turbomachinery, over and above the amount required for the rocket combustion chamber. The excess propellants are then vented overboard with a minimal contribution to thrust. In an RBCC vehicle, the possibility also exists that additional propellants would be carried on-board for cooling of vehicle surfaces. However, in this system the secondary flow is being routed back into the engine flow path in an attempt to make the engine more efficient by increasing the base pressure.

The specific impulse efficiencies for both the full-flow and gas generator were calculated from the following expression:

$$\eta_{Isp} = \frac{Isp_{CFD}}{Isp_{isentropic}} \qquad (15)$$

Tables V and VI present the full-flow and gas generator efficiencies based on isentropic performance from the CFD experiments for both the Spalart-Allmaras and k–ε turbulence models.

TABLE V.—SPECIFIC IMPULSE EFFICIENCY RESULTS WITH THE
SPALART-ALLMARAS TURBULENCE MODEL

Case	CFD Isp (sec)	Isp Isentropic Full-Flow (sec)	Isp Isentropic Full-Flow Efficiency	Isp Isentropic Gas-Generator (sec)	Isp Isentropic Gas-Generator Efficiency
1	399.54	451.58	88.48%	418.13	95.56%
2	424.33	451.58	93.97%	451.58	93.97%
3	415.94	480.05	86.65%	480.05	86.65%
4	361.73	465.07	77.78%	465.07	77.78%
5	411.29	465.07	88.44%	430.62	95.51%
6	430.64	480.05	89.71%	444.49	96.89%
7	374.07	445.44	83.98%	412.23	90.70%
8	416.89	445.44	93.59%	445.44	93.59%
9	418.36	468.03	89.37%	450.03	92.94%

Case	CFD Isp (sec)	Isp Isentropic Full-Flow (sec)	Isp Isentropic Full-Flow Efficiency	Isp Isentropic Gas-Generator (sec)	Isp Isentropic Gas-Generator Efficiency
1	410.42	451.58	90.89%	418.13	98.16%
2	427.06	451.58	94.57%	451.58	94.57%
3	415.88	480.05	86.63%	480.05	86.63%
4	373.85	465.07	80.39%	465.07	80.39%
5	425.22	465.07	91.43%	430.62	98.75%
6	437.21	480.05	91.08%	444.49	98.36%
7	375.30	445.44	84.25%	412.23	90.99%
8	418.70	445.44	94.00%	445.44	94.00%
9	423.38	468.06	90.46%	450.06	94.08%

The results from the MLR analysis are presented in Tables VII to X along with the corresponding parametric equations. Two results are reported for each data set, the estimated coefficients for a linear model and the confidence level for that value. Also included are the error estimates for each analysis. The confidence levels are the estimated probabilities that the coefficients are different from zero. A value that had a confidence level less than 90% was considered not statistically significant and dropped from the model.

Table VII presents the MLR results for the isentropic full-flow solution with the Spalart-Allmaras turbulence model.

TABLE VII.—MULTIPLE LINEAR REGRESSION FOR ISENTROPIC FULL-FLOW SOLUTION
WITH THE SPALART-ALLMARAS TURBULENCE MODEL
$[R^2 = 0.962, S_{yx} = 1.36, t = 2.132, E = \pm2.90\%]$

Term		Coefficient	Confidence Level
Constant	β_0	87.999	>99.99%
Chamber Pressure	β_1		NSS
Secondary Flow	β_2		NSS
Mixer-ejector inlet area ratio	β_3	-2.180	98.95%
Mixer-ejector length-to-diameter ratio	β_4	-1.465	96.19%
Mixer-ejector area ratio	β_5	1.878	98.26%
Rocket area ratio	β_6	3.603	99.83%

The resulting expression (16) is:

$$\eta_{Isp\text{-}FF\text{-}SA} = 87.999 - 2.180\left[\frac{\frac{A_3}{A^*} - 120}{80}\right] - 1.465\left[\frac{\frac{L}{D_3} - 3.5}{1.5}\right] + 1.878\left[\frac{\frac{A_6}{A_3} - 1.5}{0.5}\right] + 3.603\left[\frac{\varepsilon_r - 12}{8}\right]$$

The most significant effect, at 99.83% confidence, for the isentropic full-flow is the initial rocket area ratio. The results from the model coefficients can be shown graphically by using the design median point, case 9, as the default. In figure 9, the performance increases as a function of rocket area at a slope which corresponds to the model coefficient. The secondary flow and the chamber pressure were found to be not statistically significant (NSS) for this case. Decreases in performance result from increased mixer-ejector inlet area ratio and increased mixer-ejector length-to-diameter ratio, figures 10 and 11 respectively. Mixer-ejector area ratio had a positive effect on performance, as shown in figure 12. A discussion on the physical explanation of the affects of each parameter can be found later in this section.
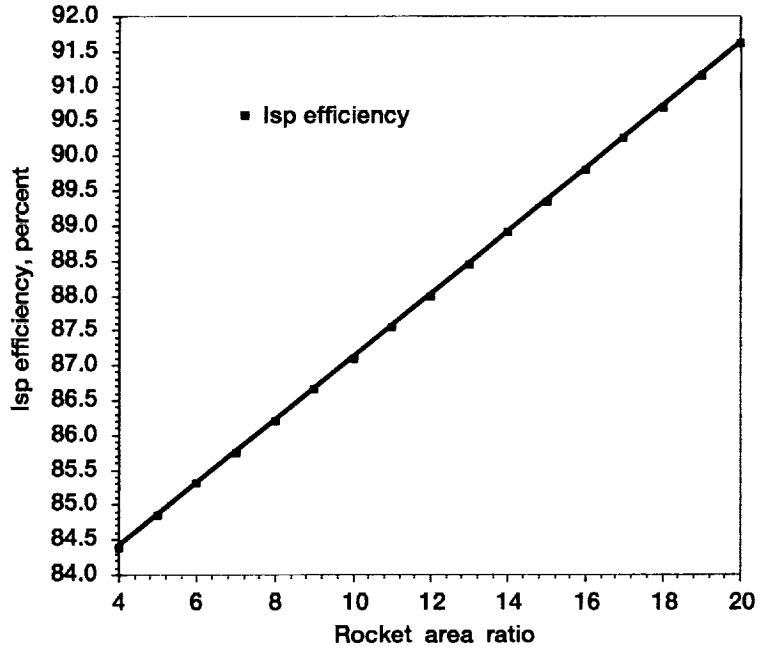
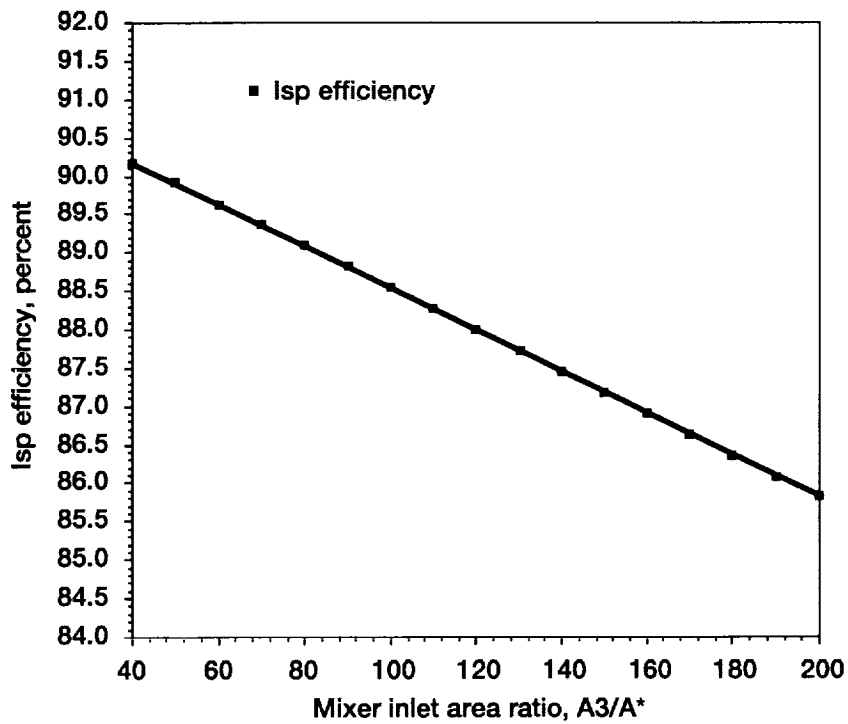Figure 9.—Affect of mixer inlet area ratio on Isp efficiency (baseline: Pc = 750 psia, Ws = 4%, A3/A* = 120, L/D3 = 3.5, A6/A3 = 1.5, Er = 12).

Figure 10.—Affect of mixer inlet area ratio on Isp efficiency (baseline: Pc = 750 psia, Ws = 4%, A3/A* = 120, L/D3 = 3.5, A6/A3 = 1.5, Er = 12).
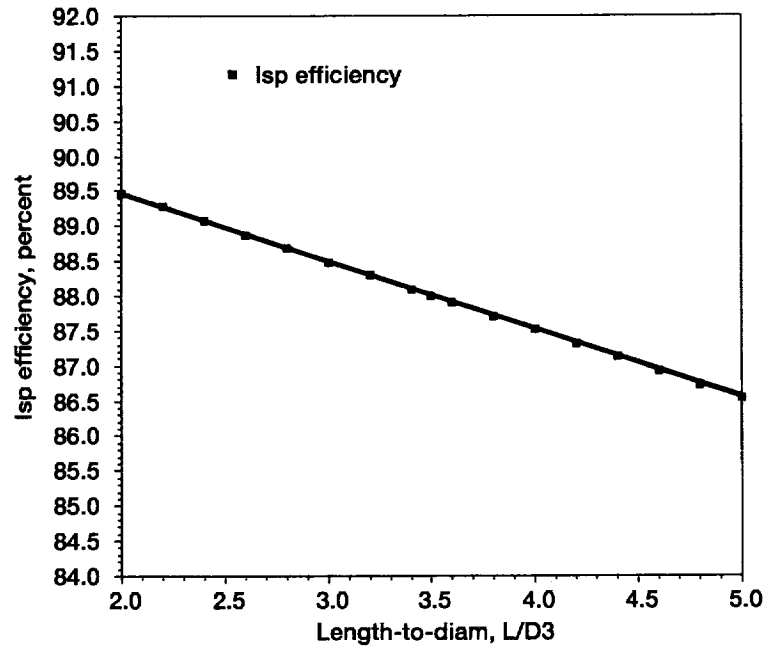
Figure 11.—Affect of length-to-diameter ratio on Isp efficiency
(baseline: Pc = 750 psia, Ws = 4%, A3/A* = 120, L/D3 = 3.5,
A6/A3 = 1.5, Er = 12).
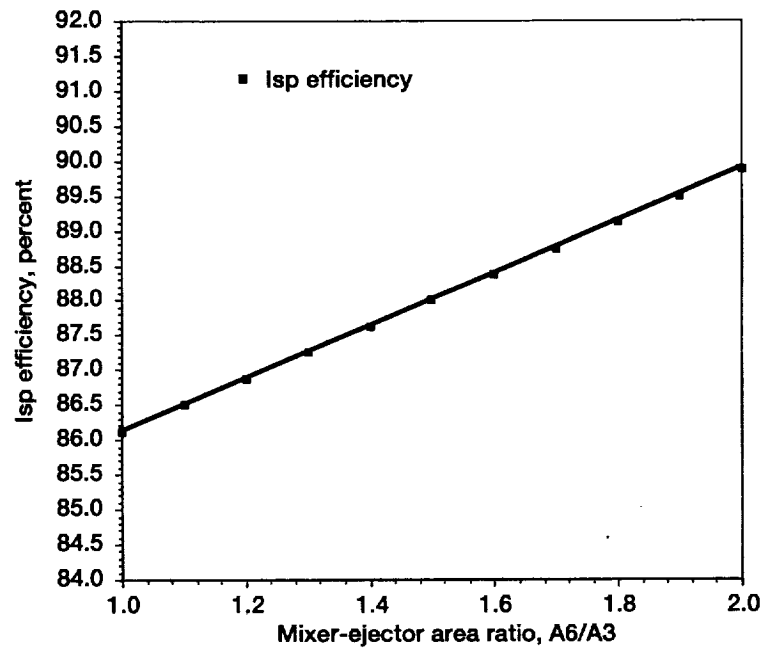

Figure 12.—Affect of mixer-ejector area ratio on Isp efficiency
(baseline: Pc = 750 psia, Ws = 4%, A3/A* = 120, L/D3 = 3.5,
A6/A3 = 1.5, Er = 12).

Table VIII presents the MLR results for the isentropic gas generator solution with the Spalart-Allmaras turbulence model.

TABLE VIII.—MULTIPLE LINEAR REGRESSION FOR ISENTROPIC GAS GENERATOR
ANALYSIS WITH THE SPARLART-ALLMARAS TURBULENCE MODEL
[$R^2 = 0.9769$, $S_{yx} = 1.486$, $t = 2.353$, $E = \pm3.50\%$]

Term		Coefficient	Confidence Level
Constant	β_0	91.512	>99.99%
Chamber Pressure	β_1		NSS
Secondary Flow	β_2	3.334	99.21%
Mixer-ejector inlet area ratio	β_3	–2.124	97.27%
Mixer-ejector length-to-diameter ratio	β_4	–1.496	93.47%
Mixer-ejector area ratio	β_5	1.936	96.54%
Rocket area ratio	β_6	3.659	99.39%

The resulting expression (17) is:

$$\eta_{\text{Isp-GG-SA}} = 91.512 + 3.334\left[\frac{ms-4}{4}\right] - 2.124\left[\frac{\frac{A_3}{A*}-120}{80}\right] - 1.496\left[\frac{\frac{L}{D_3}-3.5}{1.5}\right] + 1.936\left[\frac{\frac{A_6}{A_3}-1.5}{0.5}\right] + 3.659\left[\frac{\varepsilon_r-12}{8}\right]$$

The two most significant effects, at over 99% confidence, for the isentropic gas generator are the percent of secondary flow and the initial rocket area ratio. Increasing both of these values has a strong effect on increasing the efficiency. The system chamber pressure was found to be not statistically significant. Decreases in performance result from increased mixer-ejector inlet area ratio and mixer-ejector length-to-diameter ratio, however the confidence levels were weak. Mixer-ejector area ratio had a positive effect on performance, this is also a weak effect.

Table IX presents the MLR results for the isentropic full-flow solution with the k–ε turbulence model.

TABLE IX.—MULTIPLE LINEAR REGRESSION FOR ISENTROPIC FULL-FLOW SOLUTION
WITH THE k–ε TURBLENCE MODEL
[$R^2 = 0.9868$, $S_{yx} = 0.758$, $t = 2.132$, $E = \pm1.62\%$]

Term		Coefficient	Confidence Level
Constant	β_0	89.300	>99.99%
Chamber Pressure	β_1		NSS
Secondary Flow	β_2		NSS
Mixer-ejector inlet area ratio	β_3	–1.773	99.73%
Mixer-ejector length-to-diameter ratio	β_4	–1.583	99.59%
Mixer-ejector area ratio	β_5	1.638	99.64%
Rocket area ratio	β_6	3.615	99.98%

The resulting expression (18) is:

$$\eta_{\text{Isp-FF-k}\varepsilon} = 89.300 - 1.773\left[\frac{\frac{A_3}{A*}-120}{80}\right] - 1.583\left[\frac{\frac{L}{D_3}-3.5}{1.5}\right] + 1.638\left[\frac{\frac{A_6}{A_3}-1.5}{0.5}\right] + 3.615\left[\frac{\varepsilon_r-12}{8}\right]$$

As can be seen, the significant model coefficients are the same as those found in the SA analysis. However, the constant coefficient is slightly higher than the SA model and the confidence levels are high for all parameters determined to be significant. In this set, both chamber pressure and secondary flow are not significant parameters which affect performance. However, the four remaining items were all deemed very significant at levels of over 99.5%. Increasing mixer-ejector inlet area ratio and length-to-diameter ratio were

found to decrease performance. Increasing mixer-ejector area ratio and rocket area ratio were found to increase performance.

Table 10 presents the MLR results for the isentropic gas generator solution with the k–ε turbulence model.

TABLE X.—MULTIPLE LINEAR REGRESSION FOR ISENTROPIC GAS GENERATOR ANALYSIS WITH THE k–ε TURBULENCE MODEL
[$R^2 = 0.993$, $S_{y,x} = 0.829$, $t = 2.353$, $E = \pm 1.95\%$]

Term		Coefficient	Confidence Level
Constant	β_0	92.881	>99.99%
Chamber Pressure	β_1		NSS
Secondary Flow	β_2	3.834	99.90%
Mixer-ejector inlet area ratio	β_3	–1.699	98.98%
Mixer-ejector length-to-diameter ratio	β_4	–1.654	98.90%
Mixer-ejector area ratio	β_5	1.699	98.98%
Rocket area ratio	β_6	3.689	99.89%

The resulting expression (19) is:

$$\eta_{Isp\text{-}GG\text{-}k\varepsilon} = 92.881 + 3.834\left[\frac{\dot{m}_s - 4}{4}\right] - 1.699\left[\frac{\frac{A_3}{A^*} - 120}{80}\right] - 1.654\left[\frac{\frac{L}{D_3} - 3.5}{1.5}\right] + 1.699\left[\frac{\frac{A_6}{A_3} - 1.5}{0.5}\right] + 3.689\left[\frac{\varepsilon_r - 12}{8}\right]$$

As can be seen, the significant model coefficients are the same as those found in the SA analysis. However, the constant coefficient is slightly higher than the SA model and the confidence levels are high for all parameters determined to be significant. The two most significant effects, at over 99% confidence, for the isentropic gas generator are the percent of secondary flow and the initial rocket area ratio. Increasing both of these values has a strong effect of increasing the efficiency. The system chamber pressure was found to be not statistically significant. Decreases in performance result from increased mixer-ejector inlet area ratio and mixer-ejector length-to-diameter ratio, however the confidence levels were weak. Mixer-ejector area ratio had a positive effect on performance, this is also a weak effect.

DISCUSSION OF RESULTS

The MLR analysis was very similar for the full-flow and gas-generator analysis. The main difference was including secondary flow in the latter. Chamber pressure was found to be not statistically significant for either method of analysis. The results show that providing the maximum amount of rocket area ratio possible will significantly increase performance. This result is not unexpected and consistent with the results of figure 3 which shows the dramatic increase in Isp for area ratios less than 100. Therefore the goal should be to maximize the rocket area ratio because it provides the steepest gains in performance. However, from an RBCC system perspective this must be balanced with how increasing rocket area ratio affects the three other modes of operation.

An increasing mixer-ejector inlet area ratio was shown to decrease performance. This parameter is directly related to the amount of free expansion present between the rocket nozzle and mixer-ejector wall. For a constant rocket area ratio, increasing A_3/A^* expands the free expansion zone and reduces the systems ability to efficiently produce thrust.

An increasing length to diameter ratio was also determined to reduce Isp efficiency. Several of the loss mechanisms shown in figure 6 are applicable to the effects of L/D_3 on performance. A longer duct will obviously produce a thicker boundary layer at the exit due to viscous forces. Also, a longer duct will have a greater number of oblique shock structures and shock induced boundary layer separations. All of these mechanisms combine to decrease performance for longer mixer-ejector sections.

A gain in performance is provided by increasing the mixer-ejector exit area ratio (A_6/A_3). As with increasing rocket area ratio, it is not unexpected that an increase in mixer-ejector area ratio increases performance. In conventional nozzle theory a perfectly axial exit flow with no divergence losses provides optimum performance so one might expect that a mixer-ejector exit area ratio of 1 would be the highest performing. However, as shown if figure 6, the flowfield is not completely axial and divergence is still present at the exit. As a result, the gains from increasing mixer-ejector area ratio are greater than any divergence losses incurred.

The full-flow and gas-generator models differ in the determination of secondary flow as a significant effect. The full-flow model does not include secondary mass flow as a significant effect. Therefore the thrust increases by the same percentage as the added mass flow and there is no net change. However, for the gas-generator flow, performance increases significantly for every percent increase in secondary flow. Obviously, routing the secondary flow back into the engine provides a greater benefit than dumping the propellants overboard.

Equations 16 to 19 can be used along with the geometric values of a given engine configurations to obtain a first-order estimate of vacuum specific impulse efficiency. That value can then be used with the ideal isentropic specific impulse, depending upon full-flow or gas-generator assumption, to determine a first-order estimate of vacuum specific impulse. The result of that analysis will then help influence the trades that must be required in a specific engine configuration to obtain acceptable performance throughout the entire trajectory. First-order models like those presented in equations 16 to 19 can also be used in a cycle study to determine the trade spaces between individual modes of operation.

The Spalart-Allmaras model predicts lower results for the same conditions than the results with the k–ε model. Both models predict the same trends associated with each parameter only at a slightly different absolute value. Table 11 compares the predicted results of each model against the actual values from the CFD results along with the approximate error term. As shown by the results, the actual values for both models agree well with the model predicted values. In general the k–ε results have a closer agreement with the predicted values, hence the lower error term (E). An analysis of variance (ANOVA) was performed to determine if the differences in results between turbulence models was statistically significant. The results show that at a 99% confidence level the difference in results between turbulence models is statistically significant. For the full flow analysis, the k–ε model predicts an average of 1.03% higher than the SA model. For the full flow analysis, the k–ε model predicts an average of 1.37% higher than the SA model. Further discussion on which turbulence model is more accurate is inappropriate until the results can be validated with experimental data.

TABLE XI.—COMPARISON OF EXPERIMENTAL RESULTS WITH MODEL PREDICTIONS

Case	Spalart-Allmaras Isentropic Full-Flow E=±2.9%		Spalart-Allmaras Isentropic Gas-Generator E=±3.5%		k–ε Isentropic Full-Flow E=±1.62%		k –ε Isentropic Gas-Generator E=±1.95%	
	Actual	*Predicted*	*Actual*	*Predicted*	*Actual*	*Predicted*	*Actual*	*Predicted*
1	88.48%	89.92%	95.56%	96.74%	90.89%	90.68%	98.16%	98.08%
2	93.97%	94.19%	93.97%	94.40%	94.57%	94.74%	94.57%	94.48%
3	86.65%	85.56%	86.65%	85.83%	86.63%	87.13%	86.63%	87.01%
4	77.78%	78.87%	77.78%	78.96%	80.39%	80.69%	80.39%	80.31%
5	88.44%	89.01%	95.51%	95.94%	91.43%	91.09%	98.75%	98.66%
6	89.71%	89.83%	96.89%	96.82%	91.08%	91.20%	98.36%	98.75%
7	83.98%	83.23%	90.70%	89.88%	84.25%	84.24%	90.99%	91.37%
8	93.59%	93.37%	93.59%	93.52%	94.00%	94.63%	94.00%	94.39%
9	89.39%	88.00%	92.96%	91.51%	90.46%	89.30%	94.08%	92.88%

CONCLUDING REMARKS

Results show that performance (Isp) of an RBCC system in rocket only operation has a significant affect on total system effective equivalent specific impulse (I*). For a given trajectory, a ±10% change in rocket Isp can have a corresponding minimum of ±7% change in total I*.

The CFD results showed several areas of concern in the flow path. These include the free expansion from the rocket nozzle to mixer-ejector wall, reflected oblique shock structures through out the flow path, shock induced boundary layer separations, thick boundary layer development at the exit, and flowfield divergence at the exit. CFD particle trace results did show that injected secondary flow did alter the free expansion angle of the rocket plume along with reducing the recirculation zone.

Results from the linear regression analysis provided information on which parameters affect performance and if the effects are positive or negative. Results were similar for both the gas generator and full-flow analysis:

- Increasing mixer-ejector inlet area ratio decreases specific impulse efficiency.
- Increasing mixer-ejector length-to-diameter area ratio decreases specific impulse efficiency.
- Increasing mixer-ejector area ratio increases specific impulse efficiency.
- Increasing rocket area ratio increases specific impulse efficiency.

The one difference between the models is addition of secondary flow. For the full-flow analysis the injected secondary flow was not statistically significant. However, for the gas generator analysis it was found that increasing injected secondary flow increased the specific impulse efficiency.

The parametric equations developed provide an analysis tool to evaluate the mode 4 performance of an RBCC engine and a tool for use in total engine system trade studies. Results for the models agree well with the corresponding experimental CFD values.

Statistical differences were also determined based upon selection of turbulence model. The k-ε model was found to result in values of slightly higher specific impulse efficiencies than those calculated with the Spalart-Allmaras model. Further discussion on which turbulence model is more accurate is inappropriate until the results can be validated with experimental data.

This study has shown that utilizing design of experiments is an effective tool to maximize results while reducing the number of analytical cases required.

ACKNOWLEDGMENTS

REFERENCES

1. Escher, W.J.D.; Teeter, R.R.; and Rice, E.E.: Airbreathing and Rocket Propulsion Synergism: Enabling Measures for Tomorrow's Orbital Transports. AIAA 86–1680, June 1986.
2. Kors, D.L.: Combined Cycle Propulsion for Hypersonic Flight. IAF- 87–263, October 1987.
3. Foster, R.W.; Escher, W.J.D.; and Robinson, J.W.: Studies of an Extensively Axisymmetric Rocket Based Combined Cycle (RBCC) Engine Powered SSTO Vehicle. AIAA 89–2294, July 1989.
4. Lepsch Jr., R.A.; and Naftel, J.C.: The Performance of a Winged Booster Powered by Combined Rocket and Airbreathing Propulsion. AIAA 92–3500, July 1992.
5. Escher, W.J.D.; and Czysz, P.A.: Rocket-Based Combined Cycle Powered Spaceliner Concept. IAF–93–S.4.478, October 1993.
6. Escher, W.J.D.; Hyde, E.H.; and Anderson, D.M.: A User's Primer for Comparative Assessments of All-Rocket and Rocket-Based Combined-Cycle Propulsion Systems for Advanced Earth-to-Orbit Space Transport Applications. AIAA 95–2472, July 1995.
7. Bulman, M.; and Siebenhaar, A.: The Strutjet Engine: Exploding the Myths Surrounding High Speed Airbreathing Propulsion. AIAA 95–2475, July 1995.
8. Daines, R.L.; and Merkle, C.L.: Computation Fluid Dynamics Modeling of Rocket Based Combined Cycle Engine Flowfields. AIAA 94–3327, June 1994.
9. Rao, G.V.R.: Optimum Thrust Performance of Contoured Nozzles. Chemical Propulsion Information Agency, JANAF Liquid Propellant Group 1st Meeting, November 1959, pp. 243–259.
10. Tuttle, J.L.; and D.H. Blount: Perfect Bell Nozzle Parametric and Optimization Curves. NASA RP–1104, 1983.
11. Anon., NPARC User's Guide Version 3.0, the NPARC Alliance, September 1996.
12. Olds, J.D.: A Conceptual Design Tool for RBCC Engine Performance Analysis. AIP Proceedings of the 1997 Space Technology & Applications International Forum (STAIF–97), January 1997.
13. Olds, J.R.: Results of a Rocket-Based Combined-Cycle SSTO Design Using Parametric MDO Methods. SAE 941165, April 1994.
14. Huzel, D.K. and Huang, D.H.: *Design of Liquid Propellant Rocket Engines, Second Edition*. NASA SP–125, 1971.
15. Gordon, S.; and McBride, B.J.: *Computer Program for Calculation of Complex Chemical Equilibrium Compositions, Rocket Performance, Incident and Reflected Shocks, and Chapman-Jouguet Detonations*. NASA SP–273, 1971.
16. Siebenhaar, A; and Bulman, M.J.: The Strutjet Engine: The Overlooked Option For Space Launch. AIAA 95–3124, July 1995.
17. Pavli, A.J.; Kacynski, K.J; and Smith, T.A.: Experimental Performance of a High-Area-Ratio Rocket Nozzle. NASA TP–2720, 1987.

18. Jankovsky, R.J.; Kazaroff, J.M.; and Pavli, A.J.: Experimental Performance of a High-Area-Ratio Rocket
    Nozzle at High Combustion Chamber Pressure. NASA TP–3576, 1996.
19. Hosack, G.A., and Stromsta, R.R.: Performance of the Aerobell Extendible Rocket Nozzle. *Journal of
    Spacecraft and Rockets*, Vol. 6, No. 12, December 1969, pp. 1416–1423.
20. Nickerson, G.R.; Dang, A.L.; and Dunn, S.S.: The Rao Method Optimum Nozzle Contour Program.
    NAS8–36863, 1988.
21. Spalart, P.R.; and Allmaras, S.R.: A One-Equation Turbulence Model for Aerodynamic Flows.
    AIAA 92–0439, 1992.
22. Chien, K.-Y.: Predictions of Channel and Boundary Layers with a Low-Reynolds-Number Turbulence
    Model. *AIAA Journal*, Vol. 20 no.1, 1982, pp. 33-38.
23. Sarkar, S., Erlbacher, G., Hussaini, M.Y., and Kreiss, H.O.: The Analysis and Modeling of Dilatation
    Terms in compressible turbulence, *Journal of Fluid Mechanics*, Vol. 227, 1991, pp. 473–493.
24. Steffen, C.J.; Smith, T.D.;Yungster, S.; and Keller, D.J.: Rocket Based Combined Cycle Analysis Using
    NPARC. AIAA 98-0954 , January 1998.
25. Beyer, W.H., editor: *CRC Standard Mathematical Tables, 28th Edition*. CRC Press, Inc., 1987.

REPORT DOCUMENTATION PAGE

Form Approved
OMB No. 0704-0188

1. AGENCY USE ONLY (Leave blank)	2. REPORT DATE March 1998	3. REPORT TYPE AND DATES COVERED Technical Memorandum

4. TITLE AND SUBTITLE

Performance of an Axisymmetric Rocket Based Combined Cycle Engine During Rocket Only Operation Using Linear Regression Analysis

5. FUNDING NUMBERS

WU–242–72–01–00

6. AUTHOR(S)

Timothy D. Smith, Christopher J. Steffen, Jr., Shaye Yungster, and Dennis J. Keller

7. PERFORMING ORGANIZATION NAME(S) AND ADDRESS(ES)

National Aeronautics and Space Administration
Lewis Research Center
Cleveland, Ohio 44135–3191

8. PERFORMING ORGANIZATION REPORT NUMBER

E–11090

9. SPONSORING/MONITORING AGENCY NAME(S) AND ADDRESS(ES)

National Aeronautics and Space Administration
Washington, DC 20546–0001

10. SPONSORING/MONITORING AGENCY REPORT NUMBER

NASA TM—1998-206632

11. SUPPLEMENTARY NOTES

12a. DISTRIBUTION/AVAILABILITY STATEMENT

Unclassified - Unlimited
Subject Category: 20   Distribution: Nonstandard

This publication is available from the NASA Center for AeroSpace Information, (301) 621–0390.

12b. DISTRIBUTION CODE

13. ABSTRACT (Maximum 200 words)

The all rocket mode of operation is shown to be a critical factor in the overall performance of a rocket based combined cycle (RBCC) vehicle. An axisymmetric RBCC engine was used to determine specific impulse efficiency values based upon both full flow and gas generator configurations. Design of experiments methodology was used to construct a test matrix and multiple linear regression analysis was used to build parametric models. The main parameters investigated in this study were: rocket chamber pressure, rocket exit area ratio, injected secondary flow, mixer-ejector inlet area, mixer-ejector area ratio, and mixer-ejector length-to-inlet diameter ratio. A perfect gas computational fluid dynamics analysis, using both the Spalart-Allmaras and k-ε turbulence models, was performed with the NPARC code to obtain values of vacuum specific impulse. Results from the multiple linear regression analysis showed that for both the full flow and gas generator configurations increasing mixer-ejector area ratio and rocket area ratio increase performance, while increasing mixer-ejector inlet area ratio and mixer-ejector length-to-diameter ratio decrease performance. Increasing injected secondary flow increased performance for the gas generator analysis, but was not statistically significant for the full flow analysis. Chamber pressure was found to be not statistically significant.

14. SUBJECT TERMS

Rocket based combined cycle; Computational fluid dynamics; Rocket nozzles; Specific impulse

15. NUMBER OF PAGES
26

16. PRICE CODE
A03

17. SECURITY CLASSIFICATION OF REPORT Unclassified	18. SECURITY CLASSIFICATION OF THIS PAGE Unclassified	19. SECURITY CLASSIFICATION OF ABSTRACT Unclassified	20. LIMITATION OF ABSTRACT